International Journal of Nanoelectronics and Materials
Volume 14 (Special Issue) December 2021 [199-206]

Synthesis Methods of Tin Oxide as Photoanode for Dye-Sensitized Solar Cell Performance: A Short Review

Siti Norhafizah Idris[1,2], Mohd Natashah Norizan[1,2,a*], Ili Salwani Mohamad[1,2], Norsuria Mahmed[1,3,b*], Kaiswariah Magiswaran[1,2] and Sharizal Ahmad Sobri[1,4].

[1]Geopolymer & Green Technology, Centre of Excellence (CEGeoGTech), Universiti Malaysia Perlis (UniMAP), Perlis, Malaysia.
[2]Faculty of Electronic Engineering Technology, Universiti Malaysia Perlis (UniMAP), Perlis, Malaysia.
[3]Faculty of Chemical Engineering Technology, Universiti Malaysia Perlis (UniMAP), Perlis, Malaysia.
[4]Advanced Material Research Cluster, Faculty of Bioengineering and Technology, Universiti Malaysia Kelantan, Jeli Campus, Kelantan, Malaysia.

ABSTRACT

This review focused on the synthesis methods of tin oxide (SnO_2) nanoparticles as a photoanode for dye-sensitized solar cell (DSSC) and how it impacts the performance. There are many different techniques and various nanoparticles were produced and usually characterized by X-ray diffraction (XRD) to determine crystalline structure of SnO_2, scanning electron microscopy (SEM) to examine the surface morphology and size details and J-V solar simulator to verify current-voltage characteristics. In summary, considering all the methods reviewed, sol-gel is reported as the best method to produce SnO_2 nanoparticles for DSSC fabrication with the highest efficiency recorded of 3.96%.

Keywords: Dye-Sensitized Solar Cell (DSSC), Tin Oxide (SnO_2), synthesis, nanoparticles, characterization

1. INTRODUCTION

Sunlight is the most plentiful, cleanest, cheapest and safest energy source [1]. Photovoltaic (PV) cells are devices that convert sunlight into electricity [2]. There are three generations of photovoltaic cell technologies. The first generation dominated the PV market and is made up of monocrystalline and polycrystalline silicon [3]. The second-generation PV cells are non-crystalline silicon, copper gallium indium selenide and cadmium telluride (CdTe) [4]. The third-generation include dye-sensitized solar cells (DSSC) [5,6], quantum dots [7], organic and perovskite solar cells. DSSC has gotten a lot of interest [8] and it has also been under much scrutiny for the last three decades [9,10].

DSSC comprises the components as shown in Figure 1: (i) a transparent conductive layer of fluorine-doped tin oxide (FTO) or indium tin oxide (ITO) has been applied to a glass or plastic substrate, (ii) semiconductor oxide with a mesostructured and a large band-gap, (iii) dye sensitizer, (iv) redox mediator electrolyte, (v) counter electrode, FTO or ITO coated substrate and a thin catalyst coating [10,11]. Wide bandgap semiconducting photoanodes play a critical role in dye-sensitizer uptake and electron transport in DSSC functioning [13,14]. Tin oxide (SnO_2) has been extensively studied because of its larger band gap (3.6 eV), high electron mobility (100-200 $cm^2V^{-1}s^{-1}$), and low effective mass in the conduction band (0.1 m_0) [15] to solar cells [16], lithium-ion batteries [17], gas sensors and other applications [18].

[a*]mohdnatashah@unimap.edu.my, [b*]norsuria@unimap.edu.my

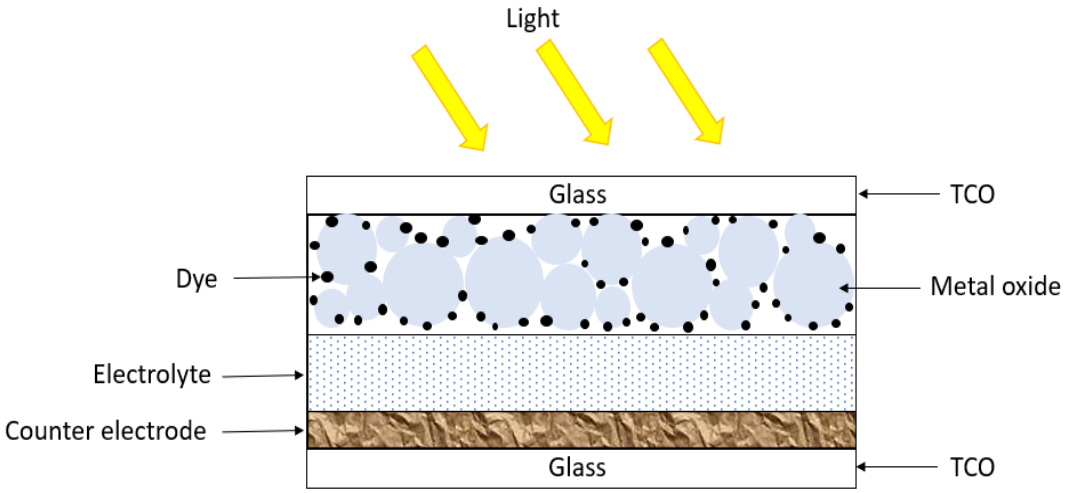

Figure 1. Basic Component of DSSC [19]

The primary function of semiconductor oxide layers is to form strong bonds with the dye molecules and to accept the photo-excited electrons from dyes. However, some circumstances must be met in order for a semiconductor oxide layer to be efficient: (i) a large area of the surface to facilitate adsorption of dyes for incredible light-harvesting, (ii) the amount of photon loss need to be kept to a minimum and be precise to the visible light, (iii) assist conduction band that is less than dye lowest unoccupied molecular orbitals (LUMO) and allow photogenerated electrons to be inserted appropriately, (iv) electron mobility must be high for effective electron transport, (v) hydroxyl groups or defects must be present in order for the dye molecule to be attached to the surface, (vi) it ought to be simple to make, stable, low-cost and environmentally friendly [11,19].

This review aims to explore the methods to prepare SnO_2 nanoparticles based on the previous researchers [8]. A variety of physical and chemical methods for fabricating various types of SnO_2 nanostructures have already been reported in the literature, including hydrothermal method [21], solvothermal [22], microwave synthesis [23], co-precipitation method, sol-gel [24], spray pyrolysis [25] and others. In addition, there has been a significant amount of effort put into developing nanostructured SnO_2 with various morphologies. As a result, a wide range of nanostructured SnO_2 materials, including nanosheets [26], nanofibers [27], nanoflowers, and hollow microspheres [28] have been synthesized and extensively studied in the context of DSSC.

2. FABRICATION OF DSSC

In preparation for working electrode (WE), tin oxide paste was applied on the FTO/ITO glass that was already covered with scotch tape by using a simple doctor blade technique, as shown in Figure 2. Annealed the glass plate in an oven at 450°C for 30 minutes. For the preparation of Ruthenium (Ru N719) dye solution, about 10 mg of Ru N719 powder was mixed with the 25 ml of ethanol solution in a volumetric flask. The flask was sealed and covered with aluminum foil to prevent light penetration. The annealed electrode was then soaked in Ru N719 dye for 10 minutes. Meanwhile, for the counter electrode (CE), graphite pencil was used to cover one side of the glass surface with a carbon film. Annealed the electrode in the oven at 450°C for 30 minutes and washed with ethanol. Next the cathode was being placed on top of the glass coated with the dye. Sandwiched the working electrode and counter electrode together and secured them. The electrolyte was filled into the space between the two electrodes and the DSSC sample was connected to a multi-meter using wires and alligator clips. The cell was placed under the light source and recorded the highest voltage and current that the solar cell can produce [7,34].

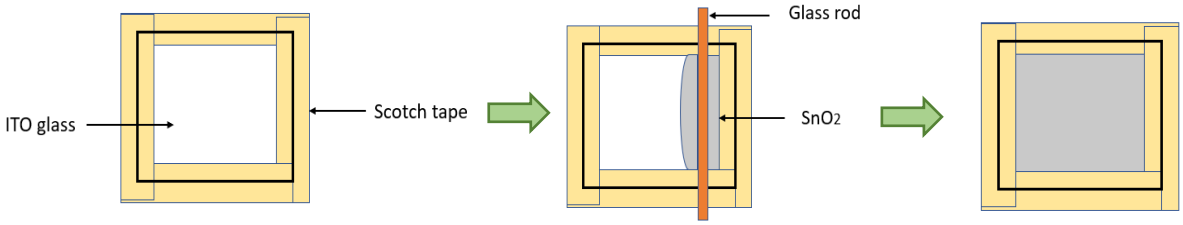

Figure 2. Doctor Blade Technique [30]

3. CHARACTERIZATION

X-ray Powder Diffraction (XRD) analysis is a popular method for determining synthesized nanomaterials' crystallinity and phase purity [16]. Using XRD patterns as a source of information, the characteristic of samples' diffraction peaks was evidently broad when the temperature is low, indicating that the small-sized nanocrystalline SnO_2 was formed. Furthermore, the shape peaks indicate that the samples may be highly crystallized [31]. Simultaneously, when the calcination temperature increased, the characteristic SnO_2 diffraction peaks grew sharper, indicating that the particle size of SnO_2 increased [32]. The Scherrer equation (equation 1) was used to estimate the average particle size (D) [33]:

$$D = \frac{0.9\lambda}{\beta\cos\theta} \tag{1}$$

Where D is crystallite size, λ is X-ray wavelength, β is diffraction peak's full width at half maximum, and θ is the Bragg diffraction angle of the diffraction peaks [21].

Scanning electron microscopy (SEM) analysis was performed to determine the size and shape of the synthesized SnO_2 nanoparticles and morphology and elemental analysis. Prior to performing the analysis, sample preparation might be complex or straightforward, depending on the samples' conductivity and the data sought. For simple preparation, acquisition of a sample that will fit inside the SEM chamber, and necessary accommodation to prevent charge build-up on electrically insulating materials are the only requirements [16].

Moreover, a variety of factors influences the optical characteristics of semiconductor materials. In general, the energy gap is the most critical factor in photocatalytic activities. Its optical properties were tested using UV-Vis spectrophotometry [16]. The optical absorption gets higher as the wavelength gets shorter [21]. Due to energy gap is the main factor in optical properties, the inverse relationship between the optical absorption and the wavelength are related with the equation 2:

$$E = \frac{hc}{\lambda} \tag{2}$$

Where E is energy, h is Planck's constant, c is the speed of light and λ is wavelength.

DSSC is characterized by the current density-voltage (J-V) curve as in Figure 4. From the curve, when the cell is short-circuited under illumination, there are the essential terms that are primarily examined and commonly used to determine solar cell performance. Open circuit voltage (V_{OC}) is the highest voltage accessible from a solar cell, while the net current across the device is zero. In most cases, the open-circuit voltage can be determined by calculating the difference between the donor component's HOMO and the acceptor component's LUMO, [34] as shown in Figure 3.

Theoretically, the HOMO-LUMO distinction can be linked to experimental results obtained by J-V characteristics.

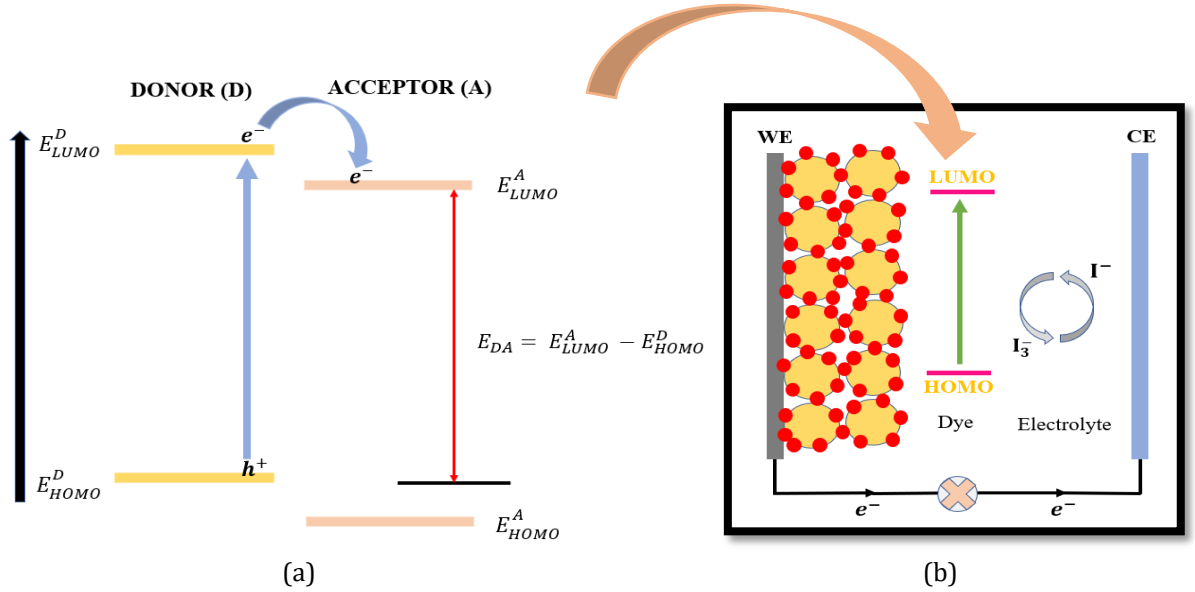

Figure 3. (a) Schematic of energy levels (b) HOMO-LUMO distinction in DSSC [42,43]

When the terminals are wired together, there is the short circuit current (I_{SC}). Since I_{SC} is usually proportional to the light intensity, when it increases, more photons and electrons are produced. Absorption of a photon with energy higher than energy band gap causing an electron to be excited in the HOMO of donor and the electron transferred to the LUMO. The electron then transported to the acceptor. Thus, I_{SC} is proportional to the solar cell's surface area, defined as short circuit current density, $J_{SC} = I_{SC}/A$. Maximum power (equation 3) generated by a cell under illumination can be obtained through the relation as follows based on Figure 4:

$$P_{max}\ (mWcm^{-2}) = \text{Fill Factor (FF)} \times J_{SC}\ (mAcm^{-2}) \times V_{OC}(V) \quad (3)$$

The ratio P_{max} to the total incident light power P_{irr} (1 sun = P_{irr} = 100 mW cm^{-2}) can be used to calculate efficiency ɳ (%) in equation 4:

$$\eta\ (\%) = (P_{max}/P_{irr}) \times 100 = (V_{OC} \cdot J_{SC} \cdot FF\ /P_{irr}) \times 100 \quad (4)$$

Usually, the FF of an organic solar cell is determined by the charge carrier mobility of holes and electrons emanating from the donor and acceptor components. Thus, solar cell devices have a greater FF if the mobility of holes and electrons is greater and in equilibrium [37].

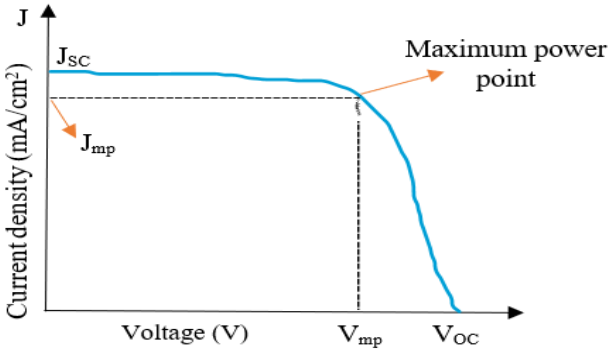

Figure 4. Performance of DSSC [38]

4. METHODS OF SYNTHESIS

4.1 Sol-gel Method

The sol-gel process begins with preparing a precursor mix (a sol or a solution) that develops materials that appear to be more solid due to evaporation of the solvent, dehydration, and chemical cross-linking between dissolved precursors and solid particles. Pure ethanol was used to dissolve hydrated tin chloride ($SnCl_2 \cdot 2H_2O$) in a typical procedure. For 30 minutes, the solution was stirred with a magnetic stirrer until a clear and solution is obtained without turbidity. Some researchers use a hydrolysis agent and also chemical modifier reagent to create a variation of SnO_2 particles. Then, the product goes through the calcination process for 1 hour at a certain temperature and SnO_2 nanoparticles were obtained [20,25,26].

4.2 Co-precipitation Route

Co-precipitation is the transport of substances that are typically soluble under the conditions used by a precipitate. A standard co-precipitation method involves dissolving tin chloride pentahydrate ($SnCl_4 \cdot 5H_2O$) in an aqueous sodium hydroxide (NaOH) solution and adjusting the pH to desired values 10. In each case, the milky white precipitate that resulted was collected, filtered, and washed several times with distilled water to eliminate contaminants, and dried for 24 hours at 80°C. Finally, the prepared SnO_2 nanopowders were annealed for 2 hours at various temperatures [8,27].

4.3 Spray Pyrolysis Technique

This method has three essential stages precursor solution composition, aerosol generation and transport, and synthesis process. Firstly, the precursor solution's chemical composition must include a substance that will produce the required chemical composition after the pyrolysis stage. The morphological properties of the final product, as well as the proper temperature range for synthesis, will be determined by the aerosol droplet size distribution and generation mechanism, in the second stage. Finally, whether the chemical reaction in the end, occurs on a heated substrate or in the gas phase determines if the synthesized substance is a powder or a film coating. The tin precursor ($SnCl_4 \cdot 5H_2O$) was dissolved in methanol in a typical synthesis. Aluminum acetylacetonate was added. The temperature for growth was set at 500°C during sample deposition, resulting in a 420°C substrate surface. This temperature was maintained for all the substrates and depositions [28,29,30].

4.4 Hydrothermal Method

The hydrothermal method involves heating and pressurizing an aqueous solution is used as a reaction system in a unique closed reaction vessel to produce a high-temperature, high-pressure reaction environment. Hydrated tin chloride ($SnCl_2 \cdot 2H_2O$) was typically dissolved in ethanol or distilled water. The solution was then transferred to a Teflon flask and autoclaved before being maintained for 12 hours in an air-flow electric oven at 180°C. After cooling to room temperature, the white precipitate was washed several times with distilled water and absolute ethanol and dried under vacuum at 80°C overnight. The finished product was annealed in the air for 2 hours at a certain temperature [31,32,33].

5. PERFORMANCE OF DSSC WITH DIFFERENT SYNTHESIS METHODS

Table 1 Performance of DSSC using Ru N719 Dye and Different Synthesis Methods of SnO_2

Synthesis Method	Sample	J_{SC} (mA/cm^2)	V_{OC} (V)	FF	η (%)	Ref.
Sol-gel method	SnO_2 nanograins	8.70	0.65	0.70	3.96	[40,41]
Co-precipitation technique	SnO_2	6.85	0.68	0.70	3.20	[27,36,42]
Spray pyrolysis technique	SnO_2	11.90	0.35	0.41	1.70	[43,44,45]
Self-assembly method	SnO_2 hollow nanospheres	8.50	0.50	0.36	1.51	[46,47]
Hydrothermal method	SnO_2 nanorods	5.50	0.44	0.59	1.40	[48,49]
	SnO_2 nanoflowers	1.50	0.53	0.50	0.32	[58]
Spin coating method	SnO_2	0.50	0.55	0.62	0.17	[59]

From Table 1, it is shown that different synthesis methods of SnO_2 can produce various nanoparticles' shapes and sizes and its effect to the DSSC efficiency. SnO_2 nanograins prepared by sol-gel method recorded the best performance compared to others. As reported in Jung-Hoon Lee et.al., sol-gel method was used to synthesis SnO_2 nanograins and increasing V_{OC} and FF were observed. Due to the enhancement of light scattering effects in nanograins, light harvesting was increased and the DSSC performance also getting higher. It has been concluded that the particles with the smallest size have the highest dye amount [47]. However, the smallest particle size did not provide the best and higher result in efficiency. If it has the most dye loading, it is likely to have many electrons from photoexcited dye molecules. The same phenomenon resulting in an increase in recombination as higher electron density rises the driving force of electrons. Nevertheless, smaller particle size entails the electrons escape to SnO_2 nanoparticles' surfaces is easier and recombining with triiodide or excited dye molecules. That could be the possible explanation for the poor performance of the lowest particle size. This case might have happened in the hydrothermal and spin coating method because the low efficiency.

6. CONCLUSION

In summary, this review covers some of the extensive work on the synthesis methods of SnO_2. Different structures of SnO_2 were synthesized via different methods, and the influence of DSSC performance was investigated. Because of its low cost, plentiful source, broad band gap, high electron mobility, and stability, SnO_2 is an attractive and reliable contender as a photoanode in DSSC application. There are various options for the technique. The sol-gel method proved it could give the best performance to synthesize SnO_2. Morphological modification is another successful strategy for improving charge transfer effectiveness by enhancing the structure's role or boosting particle surface area and interconnectivity. As a result, it can be concluded that the tactics to improve the performance of SnO_2 based DSSC do not apply exclusively to the synthesis methods of photoanode but also other DSSC components including dye, electrolyte, and counter electrode.

ACKNOWLEGEMENTS

The author would like to acknowledge the support from the Fundamental Research Grant Scheme (FRGS) under the grant number of FRGS/1/2020/TK0/UNIMAP/02/35 from the Ministry of Higher Education Malaysia and University Malaysia Perlis.

REFERENCES

[1] Z. He et al., Sci. Rep., vol **6**, (2016), pp. 6–13.
[2] Ö. Birel, S. Nadeem, and H. Duman, J. Fluoresc., vol **27**, no. 3 (2017), pp. 1075–1085.
[3] D. T. Cotfas and P. A. Cotfas, Int. J. Photoenergy, (2019).
[4] M. T. Kibria, A. Ahammed, S. M. Sony, and F. Hossain, Int. Conf. Environ. Asp. Bangladesh, (2014) pp. 51–53.
[5] D. Wei, Int. J. Mol. Sci., vol **11**, no. 3, (2010) pp. 1103–1113.
[6] T. M. W. J. Bandara et al., J. Solid State Electrochem., vol **21**, no. 6 (2017) pp. 1571–1578.
[7] K. Meng, P. K. Surolia, O. Byrne, and K. R. Thampi, J. Power Sources, vol **248**, (2014) pp. 218–223.
[8] M. M. Rashad, I. A. Ibrahim, I. Osama, and A. E. Shalan, Bull. Mater. Sci., vol **37**, no. 4 (2014) pp. 903–909.
[9] M. Grätzel, Inorg. Chem., vol **44**, no. 20 (2005) pp. 6841–6851.
[10] I. S. Mohamad, M. N. Norizan, M. K. F. M. Hanifiah, I. A. M. Amin, and M. M. Shahimin, "Fabrication and characterization of ZnO:In thin film as photoanode for DSSC using natural fruit dyes," in AIP Conference Proceedings, vol **1660**, (2015).
[11] N. Tomar, A. Agrawal, V. S. Dhaka, and P. K. Surolia, Sol. Energy, vol **207**, (2020) pp. 59–76.
[12] N. Jamalullail, I. S. Mohamad, M. N. Norizan, N. A. Baharum, and N. Mahmed, "Short review: Natural pigments photosensitizer for (DSSC)," in IEEE Student Conference on Research and Development: Inspiring Technology for Humanity, SCOReD 2017 - Proceedings, (2018) pp. 344–349.
[13] J. Gong et al., AIP Adv., vol **5**, no. 6 (2015).
[14] N. Jamalullail, I. S. Mohamad, M. N. Norizan, N. Mahmed, and B. N. Taib, "Recent improvements on TiO and ZnO nanostructure photoanode for DSSC: A brief review," in EPJ Web of Conferences, vol **162**, (2017).
[15] Z. H. Bakr and R. Jose, Natl. Conf. Postgrad. Res. , Univ. Malaysia Pahang, (2016) pp. 220–224.
[16] O. Mukhopadhyay, S. Dhole, B. K. Mandal, F. R. N. Khan, and Y. C. Ling, Biointerface Res. Appl. Chem., vol **9**, no. 5 (2019) pp. 4199–4204.
[17] Q. Zhao, L. Ma, Q. Zhang, C. Wang, and X. Xu, J. Nanomater., vol **2015**, no. 1.
[18] S. Gorai, J. Mater. Environ. Sci, vol **9**, no. 10 (2018) pp. 2894–2903.
[19] A. N. B. Zulkifili, T. Kento, M. Daiki, and A. Fujiki, J. Clean Energy Technol., vol **3**, no. 5 (2015) pp. 382–387.
[20] Y. K. Gan, N. F. Zakaria, I. S. Mohamad, and M. N. Norizan, "The effect of ZnO photoanode solution ageing to the performance of DSSC," in AIP Conference Proceedings, vol **2203** (2020).
[21] G. E. Patil, D. D. Kajale, V. B. Gaikwad, and G. H. Jain, Int. Nano Lett., vol **2**, no. 1 (2012) pp. 2–6.
[22] E. Thamarai Selvi and S. Meenakshi Sundar, Mater. Res. Express, vol **4**, no. 7 (2017).
[23] A. K. Singh and U. T. Nakate, Adv. Nanoparticles, vol **02**, no. 01 (2013) pp. 66–70.
[24] S. Mohana Priya, A. Geetha, and K. Ramamurthi, J. Sol-Gel Sci. Technol., vol **78**, no. 2 (2016)

pp. 365–372.
[25] A. R. Paloly and M. J. Bushiri, Mater. Chem. Phys., vol **261**, (2021) pp. 124209.
[26] X. Xu et al., J. Mater. Chem. A, vol **2**, no. 1 (2014) pp. 116–122.
[27] J. Gong et al., AIP Adv., vol **5**, no. 6 (2015) pp. 1–10.
[28] A. Banik, M. S. Ansari, and M. Qureshi, ACS Omega, vol **3**, no. 10 (2018) pp. 14482–14493.
[29] K. Basu et al., Sci. Rep., vol **6**, no. March (2016) pp. 1–10.
[30] C. C. Chen and C. C. Ting, Int. J. Photoenergy, vol **2013**, (2013).
[31] M. Serhan et al., "Total iron measurement in human serum with a smartphone," AIChE Annu. Meet. Conf. Proc., (2019).
[32] S. Wang et al., J. Mol. Catal. A Chem., vol **259**, no. 1–2 (2006) pp. 245–252.
[33] E. Atkins, Elements of X-ray Diffraction, vol **29**, no. 12 (1978).
[34] F. Xu, T. T. Testo, L. Wang, and X. Zhou, Cause , Regulation and Utilization of Dye Aggregation in Dye-Sensitized Solar Cells, (2020).
[35] D. Yeboah and J. Singh, Electron., vol **6**, no. 4 (2017).
[36] S. Holliday, Y. Li, and C. K. Luscombe, Prog. Polym. Sci., vol **70**, no. March (2017) pp. 34–51.
[37] P. P. Kumavat, P. Sonar, and D. S. Dalal, Renew. Sustain. Energy Rev., vol **78**, no. April (2017) pp. 1262–1287.
[38] A. Mohamed and Y. Selim, Renew. Energy Sustain. Dev., vol **3**, no. 1 (2017) pp. 83–86.
[39] M. Aziz, S. Saber Abbas, and W. R. Wan Baharom, Mater. Lett., vol **91**, no. November 2017 (2013) pp. 31–34.
[40] A. R. Razeghizadeh, I. Kazeminezhad, L. Zalaghi, and V. Rafee, Iran. J. Chem. Chem. Eng., vol **37**, no. 2 (2018) pp. 25–32.
[41] A. E. Shalan, M. Rasly, I. Osama, M. M. Rashad, and I. A. Ibrahim, Ceram. Int., vol **40**, no. 8 PART A (2014) pp. 11619–11626.
[42] C. Falcony, M. A. Aguilar-Frutis, and M. García-Hipólito, Micromachines, vol **9**, no. 8 (2018) pp. 1–33.
[43] M. Waqas Alam, U. Khatoon, and A. Qurashi, Curr. Nanosci., vol **8**, no. 6 (2012) pp. 919–924.
[44] G. K. Deyu et al., Molecules, vol **24**, no. 15 (2019) pp. 1–16.
[45] Q. Wang et al., Ceram. Int., vol **42**, no. 14 (2016) pp. 15889–15896.
[46] Y. Duan et al., J. Mater. Chem. A, vol **3**, no. 6 (2015) pp. 3066–3073.
[47] W. M. N. M. B. Wanninayake, K. Premaratne, and R. M. G. Rajapakse, J. Nanomater., vol **2016**, no. 1 (2016).
[48] J. H. Lee, N. G. Park, and Y. J. Shin, Sol. Energy Mater. Sol. Cells, vol **95**, no. 1 (2011) pp. 179–183.
[49] J. Zhang and L. Gao, J. Solid State Chem., vol **177**, no. 4–5 (2004) pp. 1425–1430.
[50] H. Bastami and E. Taheri-Nassaj, J. Alloys Compd., vol **495**, no. 1 (2010) pp. 121–125.
[51] K. A. T. A. Perera, S. G. Anuradha, G. R. A. Kumara, M. L. Paranawitharana, R. M. G. Rajapakse, and H. M. N. Bandara, Electrochim. Acta, vol **56**, no. 11 (2011) pp. 4135–4138.
[52] D. Liyanage, R. M. G. Rajapakse, and G. R. R. A. Kumara, "Fabrication of transparent dye sensitized solar cells and improving their performances," (2011) pp. 2011.
[53] F. Gu, W. Huang, S. Wang, X. Cheng, Y. Hu, and C. Li, J. Power Sources, vol **268**, (2014) pp. 922–927.
[54] L. Chen et al., J. Power Sources, vol **272**, (2014) pp. 886–894.
[55] J. Zhang, J. Feng, Y. Hong, Y. Zhu, and L. Han, J. Power Sources, vol **257**, (2014) pp. 264–271.
[56] K. Wijeratne, J. Akilavasan, M. Thelakkat, and J. Bandara, Electrochim. Acta, vol **72**, (2012) pp. 192–198.
[57] B. Li et al., J. Alloys Compd., vol **509**, no. 5 (2011) pp. 2186–2191.
[58] R. Bhattacharjeez and I. M. Hung, ECS Solid State Lett., vol **2**, no. 11 (2013) pp. 2–6.
[59] M. Liu et al., Mater. Lett., vol **76**, (2012) pp. 215–218.